Dynamic Model of Ozone Contacting Process with Oxygen Mass Transfer in Bubble Columns

Y. H. Chen[1]; C. Y. Chang[2]; C. Y. Chiu[3]; W. H. Huang[4]; Y. H. Yu[5]; P. C. Chiang[6]; Y. Ku[7]; and J. N. Chen[8]

Abstract: The dynamic process of the dissolution of ozone in a countercurrent bubble column is studied for model establishment. Bubble columns have been used widely for ozone contacting in the plant and laboratory. Ozone is produced by oxygen-enriched gas through an ozone generator, and introduced into the bottom of the column equipped with the gas diffuser. The ozone contacting system proceeds for a temporary and unsteady period before reaching steady state. The available ozone dissolution models employed for the description of the dissolved ozone profiles were commonly developed for the steady state. Moreover, oxygen mass transfer is usually neglected in the preceding ozone dissolution models. However, this information is desirable for proper operation of ozone dissolution in a bubble column. Thus, the objective of this study is to model and investigate the dynamic ozone dissolution process in a bubble column with the oxygen mass transfer. The dynamic axial dispersion model proposed is employed to predict the variations of ozone and oxygen concentrations along the column, and the amount of off-gas. The validity of the model is demonstrated by comparing the predicted results with the experimental data. The dynamic model of ozone dissolution is useful and referable for proper prediction of the variables of the ozone contacting system in a bubble column.

Introduction

Ozone is widely used as an oxidant applied in water treatment and disinfection. It is commonly produced by electrical discharge into pure oxygen or oxygen-enriched gas through an ozone generator. The mixture of gases composed of oxygen and ozone is transferred to water by bubbling it through the bulk solution. The efficiency of ozonation processes is usually dependent on the dissolved ozone concentration. Certainly, a quantification of the dissolved ozone concentration variation is critical to the rational design and optimization of the ozonation treatment.

[1]Graduate Institute of Environmental Engineering, National Taiwan Univ., Taipei 106, Taiwan.

[2]Graduate Institute of Environmental Engineering, National Taiwan Univ., Taipei 106, Taiwan (corresponding author). E-mail: cychang3@ccms.ntu.edu.tw

[3]Dept. of Environmental Engineering, Lan-Yang College of Technology, I-Lan 261, Taiwan.

[4]Graduate Institute of Environmental Engineering, National Taiwan Univ., Taipei 106, Taiwan.

[5]Graduate Institute of Environmental Engineering, National Taiwan Univ., Taipei 106, Taiwan.

[6]Graduate Institute of Environmental Engineering, National Taiwan Univ., Taipei 106, Taiwan.

[7]Dept. of Chemical Engineering, National Taiwan Univ. of Science and Technology, Taipei 106, Taiwan.

[8]Graduate Institute of Environmental Engineering, National Chiao-Tung Univ., Hsin-Chu 300, Taiwan.

Bubble column reactors (BCRs) are commonly used in plants and laboratories for ozone contacting in the United States and throughout the world (Langlais et al. 1991). Compared to other ozone contactors, BCRs offer the advantage of the little maintenance, high liquid phase content for treatment, reasonable mass transfer rates at low-energy input, little space required, and relatively low cost (Deckwer and Schumpe 1993). Although other kinds of ozone contactors such as jet pump contactors also have higher mass transfer performance (Wright et al. 1998), BCRs are more feasible for a large liquid flow rate due to its simple geometry and construction. Bubble columns are typically constructed with 18–22 ft water depths to achieve 85–95% ozone transfer efficiency. Ozone-containing gas is introduced into the bottom of the column. The direction of the liquid flow may be cocurrent or countercurrent. Since gaseous ozone is not completely transferred into the water, the columns are covered to hold the off-gas containing the residual ozone. The off-gas from the head space of the bubble column should not be discharged into the atmosphere, since ozone is an air pollutant. Instead, gas with high-purity oxygen can be recycled to the ozone generator. Otherwise, excess ozone must be removed by a destruction process before the gas is discharged. Therefore, the excess amount and the ozone concentration of the off-gas offer valuable information for the follow-up treatment of being recycled or discharged (Masschelein 1982).

Certainly, there exists a temporary and unsteady period before the ozone contacting system reaches the steady state. The available ozone dissolution models employed for the description of the dissolved ozone profiles were commonly developed for the steady state (Mariñas et al. 1993; Zhou et al. 1994; Huang et al. 1998). Le Sauze et al. (1993) applied several models to simulate the ozone transfer in a bubble column and found that the axial dispersion model gives the best modeling of a pilot unit. Chiu et al. (1997, 2002) and Qiu et al. (2001) have studied the dynamic ozone absorption and reactions in stirred tank vessels. However, such information about the dynamic process of ozone dissolution

in bubble columns is still scarce. Accordingly, the prediction of the treating qualities of water such as the Ct_c factor in the initial stage of ozone contacting is usually not available. Also, the required duration for steady-state establishment remains to be determined. The Ct_c factor is defined as the product of the concentration of the dissolved ozone, C, in milligrams per liter, and the contact time, t_c, in minutes. The value of C would be assumed to the value at the point in the column of concern, while t_c would be assumed to the t_{10} value, where t_{10} is determined by the tracer test and equals the time necessary for 10% of the tracer mass to exit the column (Langlais et al. 1991). Furthermore, one of the advantages of ozone dissolution is its contribution to dissolved oxygen, which can be used in the biological process after the decomposition of ozone (McGhee 1991). The concentration of ozone is usually relatively low with respect to that of oxygen in the carrier gas. The oxygen mass transfer may affect the ozone concentrations of the liquid and off-gas. However, the description of the role of oxygen is usually not included in modeling the ozone dissolution. This would result not only in a lack of information of the dissolved oxygen concentration but also in an incomplete description of the ozone mass transfer during the ozone contacting processes.

The objective of this study is to model and investigate the dynamic ozone contacting process in a countercurrent bubble column with the oxygen mass transfer. Three major factors are included in the dynamic ozone contacting model: (1) hydrodynamic behavior; (2) gas–liquid mass transfer; and (3) ozone decomposition reaction kinetics. Note that the reaction kinetics of this model considers solely the decomposition of the dissolved ozone in water, which is applicable to the cases of the disinfection and oxidation with a relative small amount of impurity (Smith and Zhou 1994). For systems with a considerable amount of contaminants, the role of the contaminants should then be included in describing the ozonation kinetics and ozone consumption. This would be taken as our further work. Based on the dynamic axial dispersion model (DADM) proposed in this paper, the dynamic variations of the ozone and oxygen concentration profiles can be predicted. Further, the experimental data of the ozone dissolution in the bubble column are obtained for the model verification. Moreover, the effects of the simplified assumptions, which neglect the oxygen mass transfer or superficial gas velocity variation, on ozone dissolution simulation are examined. The validity of the model is demonstrated by the good agreement of the predicted results with the experimental data. The proposed model can provide useful information about the dynamic dissolution process of ozone in a bubble column.

Theoretical Analysis

Modeling of the dynamic processes of ozone dissolution in a bubble column requires quantification of the rates of the mass transfer and ozone decomposition reaction associated with the hydrodynamic condition of the system. Noting that the diffusivities of ozone and oxygen in the gas phase are about 10^4 times higher than those in the liquid phase, this study assumes that the resistance of the mass transfer is solely contributed by the liquid phase. As the ozone is dissolved in water, it may be consumed via the self-decomposition reaction. For spontaneous ozone decomposition to oxygen in water, the overall reaction and the corresponding pseudo-first-order decomposition rate equation may be expressed in the following forms (Kuo and Huang 1995):

$$2O_3 \rightarrow 3O_2 \tag{1}$$

$$-\frac{dC_{ALb}}{dt} = \frac{2}{3}\frac{dC_{OLb}}{dt} = k_d C_{ALb} \tag{2}$$

It is noted that Eq. (1) is an overall expression. In fact, the ozone decomposition involves a rather complex mechanism. The hydrodynamic condition of the flow field affects the concentration profiles. A dynamic axial dispersion model is developed to describe the dynamic processes of ozone dissolution in a countercurrent bubble column. The derivation of the governing equations are shown in detail in the Appendix. The resulting equations in dimensionless forms are as follows.

For the overall mass balance of the gas phase, one may have a dimensionless governing equation such as Eq. (3) for the superficial gas velocity:

$$\frac{dU_G}{d\zeta} = \frac{\alpha_P}{\beta_P}U_G - E_{rA}\mathsf{St}_{GA}\frac{1+\alpha_P}{\beta_P}y_A(\theta_{AGi}-\theta_{ALb})$$

$$-R_{fO}\mathsf{St}_{GO}\frac{1+\alpha_P}{\beta_P}y_O(\theta_{OGi}-\theta_{OLb}) \tag{3}$$

for

$$0 \leq \zeta \leq h_B^*$$

with boundary condition (BC):

$$\zeta = 0$$
$$U_G = 1 \tag{4}$$

For $h_B^* < \zeta \leq 1$, $U_G = 0$. The dimensionless height of the gas bubbles (h_B^*), which can be calculated by Eq. (5), has the maximum value of unity:

$$\frac{dh_B^*}{d\tau} = R_{uGL}U_{G,\zeta=h_B^*} \tag{5}$$

with initial condition (IC):

$$\tau = 0 \quad h_B^* = 0 \tag{6}$$

The governing equations of ozone and oxygen in gas and liquid phases are as follows. For the hold-up gases,

$$\frac{\partial\theta_{AGi}}{\partial\tau} = R_{uGL}\left[\frac{1}{\mathsf{P}_G}\frac{\partial^2\theta_{AGi}}{\partial\zeta^2} - \frac{\partial(U_G\theta_{AGi})}{\partial\zeta}\right.$$

$$\left. -E_{rA}\mathsf{St}_{GA}(\theta_{AGi}-\theta_{ALb})\right] \tag{7}$$

$$\frac{\partial\theta_{OGi}}{\partial\tau} = R_{uGL}\left[\frac{1}{\mathsf{P}_G}\frac{\partial^2\theta_{OGi}}{\partial\zeta^2} - \frac{\partial(U_G\theta_{OGi})}{\partial\zeta}\right.$$

$$\left. -R_{fO}\mathsf{St}_{GO}(\theta_{OGi}-\theta_{OLb})\right] \tag{8}$$

For the liquid phase,

$$\frac{\partial\theta_{ALb}}{\partial\tau} = \frac{1}{\mathsf{P}_L}\frac{\partial^2\theta_{ALb}}{\partial\zeta^2} + \frac{\partial\theta_{ALb}}{\partial\zeta}$$

$$+E_{rA}\mathsf{St}_{LA}(\theta_{AGi}-\theta_{ALb}) - \mathsf{Da}_A\theta_{ALb} \tag{9}$$

$$\frac{\partial\theta_{OLb}}{\partial\tau} = \frac{1}{\mathsf{P}_L}\frac{\partial^2\theta_{OLb}}{\partial\zeta^2} + \frac{\partial\theta_{OLb}}{\partial\zeta}$$

$$+R_{fO}\mathsf{St}_{LO}(\theta_{OGi}-\theta_{OLb}) + \mathsf{Da}_O\theta_{ALb} \tag{10}$$

For the gas ozone in the free volume in the column,

JOURNAL OF ENVIRONMENTAL ENGINEERING / NOVEMBER 2002 / **1037**

$$\frac{d\theta_{AGe}}{d\tau} = R_{LF} U_{G,\zeta=1}(\theta_{AGi,\zeta=1} - \theta_{AGe}) \qquad (11)$$

The ICs of Eqs. (7)–(11) are

$$\tau = 0$$

$$\theta_{AGi} = \theta_{OGi} = \theta_{ALb} = \theta_{AGe} = 0 \qquad (12)$$

$$\theta_{OLb} = \theta_{OLb0}$$

The BCs of Eqs. (7)–(10) are as follows:
    At the bottom, $\zeta = 0$:

$$\theta_{AGi} = 1 + \frac{1}{\mathsf{P}_G} \frac{\partial \theta_{AGi}}{\partial \zeta}$$

$$\theta_{OGi} = 1 + \frac{1}{\mathsf{P}_G} \frac{\partial \theta_{OGi}}{\partial \zeta}$$

$$\qquad (13)$$

$$\frac{\partial \theta_{ALb}}{\partial \zeta} = \frac{\partial \theta_{OLb}}{\partial \zeta} = 0 \qquad (14)$$

At $\zeta = h_B^*$:

$$\frac{\partial \theta_{AGi}}{\partial \zeta} = 0$$

$$\frac{\partial \theta_{OGi}}{\partial \zeta} = 0$$

$$\qquad (15)$$

$$\theta_{ALb} = -\frac{1}{\mathsf{P}_L} \frac{\partial \theta_{ALb}}{\partial \zeta}$$

$$\theta_{OLb} = \theta_{OLb0} - \frac{1}{\mathsf{P}_L} \frac{\partial \theta_{OLb}}{\partial \zeta}$$

$$\qquad (16)$$

Eqs. (3)–(16) represent the governing equations of the DADM for the two-phase contacting process of the gases (ozone and oxygen) and the liquid accompanied with liquid ozone decomposition in a countercurrent bubble column. It is worth noting the distinguished contributions of this analysis with others. The present work considers: (1) the dynamic state; (2) the oxygen mass transfer; (3) the effect of the ozone decomposition; and (4) the superficial gas velocity variation. The steady-state studies of Zhou et al. (1994) and Huang et al. (1998) considered the gas velocity variation while neglected the oxygen mass transfer ($\mathsf{St}_{GO} = \mathsf{St}_{LO} = 0$), and that of Mariñas et al. (1993) neglected the oxygen mass transfer and gas velocity variation ($\mathsf{St}_{GO} = \mathsf{St}_{LO} = 0$, $U_G = 1$). Further note that, in the present model, both the ozone decomposition and adsorption are considered as included in Eqs. (2) and (7)–(10). When E_{rA} and R_{fO} are close to unity, the gas adsorption is mainly physical. Otherwise, chemical adsorption proceeds.

Experiment

The validity of the DADM is verified by the experimental data by carrying out ozone contacting processes. Modeling equations with the corresponding ICs and BCs are solved by the finite-difference and fourth-order Runge–Kutta methods with the Turbo C program. Some values of the parameters required for the model need to be determined before solving the system equations.

Instrumentation and Materials

An airtight bubble column of 15.8 cm inside diameter made of polyvinyl chloride with an effective volume of 28.18 l is employed in this work. A solution of about 1.33 m height (L) is held in the column for all experiments, while the aspect ratio of the height to diameter is 8.42. The volume of the free space (V_F) in the bubble column is about 2.10 l. The gas diffuser of the perforated ceramic plate with a diameter and mean pore size of 10.5 cm and 28 μm is located at the bottom of the column. Ozone-containing gas generated by pure oxygen ($y_A + y_O = 1$) is introduced into the column with various gas superficial velocities ($u_{G0} = 1.33$–9.48 mm/s). The generation of ozone is controlled by the power input of the ozone generator (model FSX-0.1, Fuji, Tokyo) at constant gas pressure (98 kPa). The fed (C_{AGi0}) and discharged (C_{AGe}) gas ozone concentrations are measured by an ultraviolet (UV) photometric ozone analyzer (model SOZ-6004, Seki, Tokyo), which is calibrated by the potassium iodide (KI) titration method (Rankness et al. 1996).

A liquid-storage tank is equipped with a thermostat to maintain a constant temperature for the solution at 21°C in all experiments. Two pumps (models MD-30 RZ and MD-70 RZ, Iwaki, Tokyo) are used to transport the liquid into and out of the column with set liquid superficial velocities ($u_L = 1.42$–4.25 mm/s). A liquid ozone monitor (model 3600, Orbisphere Laboratory, Neuchàtel, Switzerland) with a sensor with membrane-containing cathode, is used to analyze the dissolved ozone concentration (C_{ALb}). The meters of the dissolved oxygen (model Oxi 340, Wissenschaftlich-Technische Werkstätten GmbH & Co. KG (WTW), Weilheim, Germany) and conductivity (model LF 340, WTW, Weilheim, Germany) with sensors of model CellOx 325 (WTW, Weilheim, Germany) and model TetraCon 325 (WTW, Weilheim, Germany) are used to measure the dissolved oxygen concentration and conductivity, respectively. The retention time of the liquid flowing from the bottom of the column to the sensors is about 12–36 s for the different u_L employed. All the recorded data are adjusted with the corresponding instrument response time (Letzel et al. 1999) of about 1–7 s and the retention time for examining the concentration variations of the effluent from the column.

At the top, the pressure transmitter (model 691, Huba, Würenlos, Switzerland) with a range of 0–30 kPa is used to measure the gas pressure (P_T) of the free space. At the middle (z_M), a differential pressure transmitter (model 692, Huba, Würenlos, Switzerland) with a range of 0–10 kPa is employed to detect the pressure difference ($P_{Z_M} - P_T$) for computing the liquid height. At the bottom, a model ST 3000 differential pressure transmitter (Honeywell, Phoenix, AZ) with a range of 0–2 kPa is used to give the pressure difference (ΔP) of two points [with hydrostatic height (h_s)] with and without aeration. The gas holdup (ε_G) is then estimated by the differential hydrostatic pressure method employing $\varepsilon_G = \Delta P/[(\rho_L - \rho_G)gh_s]$ (Shetty et al. 1992).

All experimental solutions are prepared using deionized water without other buffers. The conductivity of the water used is less than 1 μs/cm. The measured value of pH during ozone contacting in the bubble column is about 6.3 ± 0.3. The initial dissolved oxygen concentration (C_{OLb0}) in the experiments is close to the saturated value in equilibrium with air as $\theta_{OLb0} = 0.21/[P_T(1 + \alpha_P)y_O]$. For example, $0.21/[P_T(1+\alpha_P)y_O] = 0.190$, at $P_T = 1$ atm, $y_O = 0.984$, and $\alpha_P = 0.124$, while the measured θ_{OLb0} [$= C_{OLb0}/(C_{OGi0}/H_O)] = 0.187$ ($C_{OLb0} = 8.9$ mg/L, with $C_{OGi0} = 1468$ mg/L, $H_O = 30.81$).

Experimental Procedures

There have been numerous studies about the mixing effect on the performance of bubble columns, for example, those of Levenspiel (1972), Deckwer et al. (1974), Rice et al. (1981), Shah et al. (1982), Langlais et al. (1991), Deckwer and Schumpe (1993), and

Table 1. Summary of Hydrodynamic and Mass Transfer Properties at Various Superficial Gas (u_{G0}) and Liquid (u_L) Velocities; Inlet Gas: Pure Oxygen, $L = 1.33$ m, temp. $= 294$ K

u_{G0} (mm/s)	u_L (mm/s)	E_L (m^2/s)	t_L (s)	$k^0_{LO}a$ (s^{-1})	ε_G (—)	$k^0_{LA}a$ (s^{-1})
1.33	1.42	0.00855	934	0.00664	0.00435	0.00588
1.33	2.83	0.00856	467	0.00682	0.00419	0.00604
1.33	4.25	0.00852	311	0.00664	0.00437	0.00588
2.31	4.25	0.01254	310	0.00795	0.00863	0.00704
4.85	4.25	0.02334	307	0.01270	0.0184	0.01125
7.40	4.25	0.03261	304	0.01680	0.0285	0.01488
9.48	4.25	0.04120	302	0.01930	0.0349	0.01709

Zahradník and Fialová (1996). Their results indicate that the axial dispersion coefficient of liquid (E_L) is probably a function of u_{G0}, column diameter, solution properties, gas-diffuser design, etc. A pulse-input tracer test has been commonly conducted to examine the hydrodynamic behavior of the experimental apparatus employed. Sodium chloride (NaCl) is chosen as the liquid tracer in this work due to its low volatility and easy quantification by the conductivity measurement. The concentration and injection volume of $NaCl_{(aq)}$ used in each tracer test are 200 g/L and 11 mL, respectively. E_L can be obtained according to the residence time distribution (RTD) of the tracer. As for gas phase mixing, BCRs are often modeled with neglect of the axial dispersion of gas, since the dispersion influent of the gas phase is insignificant in the homogeneous bubbling regime (Shetty et al. 1992; Zahradník and Fialová 1996). Thus, the value of P_G for the modeling requirement in this work is chosen as high as 500 for the plug flow assumption of the gas phase.

Oxygen aeration has often been applied to study the gas–liquid mass transfer coefficient by numerous investigators because the chemical reaction in the O$_2$–liquid system can be neglected and the dissolved oxygen concentration is easily measured (Alvarez-Cuenca and Nerenberg 1981; Hikita et al. 1981; Shah et al. 1982; Deckwer et al. 1983; Letzel et al. 1999). The variation of the effluent dissolved oxygen concentration ($C_{OLb,\text{eff}}$) is monitored in this study to obtain the $k^0_{LO}a$ of oxygen in water. This approach considers the hydrodynamic condition. $k^0_{LO}a$ of oxygen can then be corrected to obtain the $k^0_{LA}a$ of ozone for the physical adsorption by $k^0_{LO}a/(k^0_{LA}a) = (D_O/D_A)^{0.5}$, according to the surface renewal theory (Danckwerts 1970; Biń 1995). The values of D_O and D_A of 2.24×10^{-9} and 1.76×10^{-9} m^2/s at 21°C are calculated from Wilke and Chang's formula (1955). Henry's constant of oxygen (H_O) is 30.81 at 21°C in water (Sawyer et al. 1994).

The values of the ozone decomposition rate constant (k_d) and Henry's constant (H_A) are obtained by batch and semibatch experiments, respectively. The temperature of the deionized water used in the stirred reactor is maintained at 21°C by a water jacket. The stirring speed is as high as 800 rpm to ensure the complete mixing of the liquid and gas phases according to previous tests. Ozone-containing gas is introduced into the reactor with a gas flow rate of 1.78 NLPM (L/min at 0°C, 1 atm). The detailed geometric size and operation conditions of the stirred reactor may be found elsewhere (Li et al. 2000; Chang et al. 2001).

Accordingly, ozone dissolution with distinct u_L, u_{G0}, and C_{AGi0} in a countercurrent bubble column is performed for the model verification. Before starting the ozone dissolution experiments, the ozone-containing gas is bypassed to the photometric analyzer to assure stability and determine the ozone concentration. A portion of the gas stream at a preset flow rate is directed into the column when reaching the set conditions. All experiments

performed to study the dynamic process of ozone dissolution are carried out until reaching steady state (ss) with concentrations of $C_{ALb,ss}$, $C_{OLb,ss}$, and $C_{AGe,ss}$.

Results and Discussion

The results concerning the dynamic ozone dissolution in bubble columns include two parts: (1) the parameter determination of the ozone contacting system; and (2) ozone dissolution experiments associated with model verification. The system parameters, including E_L, $k^0_{LO}a$, $k^0_{LA}a$, k_d, and H_A, are estimated. The ozone dissolution experiments are carried out with different inlets u_{G0}, u_L, and y_A. The temporal concentration variations of the θ_{ALb}, θ_{OLb}, and θ_{AGe} are monitored in order to provide experimental data for model verification.

Ozone Dissolution Parameters Determination

The equation describing the concentration variation of the tracer ($C_\theta = C_t Q_L t_L / m_t$) is similar to Eq. (9) with θ_{ALb} replaced by C_θ without the third and fourth terms on the right-hand side of Eq. (9). The IC is $C_\theta = 0$ at $\tau = 0$. The BCs at the bottom and top of the column are similar to Eqs. (14) and (16) of θ_{ALb} plus a pulse-input $\delta(\tau)$ on the right-hand side of Eq. (16), respectively. E_L values are obtained from the effluent RTD of the tracer (Levenspiel 1972), as listed in Table 1. It is seen that E_L is dependent slightly on u_L and strongly on u_{G0}, respectively. This finding is consistent with the conclusion of previous studies (Deckwer et al. 1974; Deckwer and Schumpe 1993).

As for oxygen aeration, Eqs. (3)–(6), (8), and (10) and their corresponding ICs and BCs are applied to describe the θ_{OLb} in the column. The values of P_L obtained in the tracer tests are used. A comparison of θ_{OLb} from the model prediction to that from the experiments then gives the proper values of $k^0_{LO}a$. The mass transfer properties ($k^0_{LO}a$, $k^0_{LA}a$, and ε_G) along with hydrodynamic characteristics (E_L and t_L) of the bubble column at various u_{G0} and u_L are listed in Table 1.

From the above results, the parameters of E_L, ε_G, and $k^0_{LO}a$ mainly depend on u_{G0}. The correlations derived from Table 1 can be expressed as: $E_L = 1.696 u_{G0}^{0.803}$, $\varepsilon_G = 5.168 u_{G0}^{1.063}$, and $k^0_{LO}a = 0.2567 u_{G0}^{0.560}$. The correlation of E_L shows $E_L \propto u_{G0}^{0.803}$, which is considered reasonable for the bubble flow regime (Rice et al. 1981). Deckwer et al. (1983) illustrated that the $k^0_{LO}a$ value is relatively independent of the liquid velocity and is about the same for various bubble columns with u_L varied from 10 to 120 mm/s. The $k^0_{LO}a$ values of 0.00664–0.0193 s^{-1} of this study in Table 1 are greater than 0.000843–0.00842 s^{-1} obtained from the correlation of Akita and Yoshida (1973). One may notice that the higher $k^0_{LO}a$ values are attributed to the difference of the gas

spargers used (Shah et al. 1982). The gas sparger of this study is porous with multipores of mean pore size of 28 μm, while that of Akita and Yoshida (1973) is a single hole 5.0 mm in diameter.

The value of k_d is computed from Eq. (2) with $\ln(C_{ALb}/C_{ALb0})$ versus t in the batch reactor. The obtained value of k_d is 1.47 $\times 10^{-4}$ s^{-1}. The rate expression of ozone decomposition can then be expressed as $-dC_{ALb}/dt = k_d C_{ALb} = 1.47 \times 10^{-4}$ s$^{-1} C_{ALb}$ with $R^2 = 0.998$. The value of k_d of 1.47 $\times 10^{-4}$ s^{-1} is small due to the low ionic strength and moderate pH value (about 6.3) of the deionized water (Staehelin and Hoigné 1982). Therefore, E_{rA} and R_{fO} computed by Eqs. (19 and 20) are about 1–1.000002 and 1–0.99993 for the conditions studied in this work, respectively. These values of E_{rA} and R_{fO} are close to unity and thus can be deemed as unity for further use. Considering the combined absorption and decomposition of ozone in a semibatch stirred gas–liquid reactor (sb), one obtains the mass balance equation, $C_{AGe,ss}/H_A = [k_d + (k_{LA}^0 a)_{sb}/\varepsilon_L]C_{ALb,ss}/[(k_{LA}^0 a)_{sb}/\varepsilon_L]$, describing the steady-state condition in the reactor for the consumption of the ozone decomposition. The $(k_{LA}^0 a)_{sb}/\varepsilon_L$ of ozone is determined as 0.0186 s^{-1} by conducting the oxygen aeration in the semibatch reactor and applying $k_{LO}^0 a/(k_{LA}^0 a) = (D_O/D_A)^{0.5}$. With the available $(k_{LA}^0 a)_{sb}/\varepsilon_L$, one may perform a linear regression by plotting $C_{AGe,ss}$ against $[k_d + (k_{LA}^0 a)_{sb}/\varepsilon_L]C_{ALb,ss}/[(k_{LA}^0 a)_{sb}/\varepsilon_L]$ at various inlet gas ozone concentrations. The slope representing the H_A is obtained as 3.802. The value of H_A is close to 4.025 derived by Langlais et al. (1991) at the same temperature. The slight difference may be caused by the difference of the pH and ionic strength of the solutions used (Sotelo et al. 1989). All the above obtained parameters (E_L, $k_{LO}^0 a$, $k_{LA}^0 a$, k_d, ε_G, and H_A) along with $H_O(= 30.81)$ are used for model prediction in bubble columns.

Ozone Dissolution in Bubble Column

The dynamic variations of the ozone and oxygen concentration profiles are predicted by solving for Eqs. (3)–(16). All input values of the modeling parameters can be obtained from the preceding results associated with the operation conditions. The simulated results of interest, including θ_{ALb}, θ_{OLb}, θ_{AGe}, and $U_{G,\zeta=1}$, would be verified with the ozone dissolution experiments. Comparative analysis is also performed to elucidate the effect of the simplified assumptions used by different investigators on the simulation results of the dynamic ozone contacting processes. The predicted results of the DADM are compared with the experimental data of the ozone dissolution from the beginning to steady state.

The experimental results of $\theta_{ALb,eff}$ and θ_{AGe} versus τ with $u_L = 1.42$ mm/s, $u_{G0} = 1.33$ mm/s, and various y_A are shown in Fig. 1 along with the model predictions of three cases. Case 1 considers (1) oxygen mass transfer, and (2) superficial gas velocity variation; case 2 neglects (1) while considering (2); and case 3 neglects both (1) and (2). The influence of y_A (0.00428–0.0191) on the model predictions is found to be negligible. Both the model predictions and experimental data of $\theta_{ALb,eff}$ and θ_{AGe} approach the steady-state values as τ is greater than 1.5. For a short time, say $\tau < 0.3$, the model predictions of the three cases are close. However, as τ becomes large, the model predictions of case 3 overestimate about 4–10% of $\theta_{ALb,eff}$ and θ_{AGe}. The difference between the predictions of cases 1 and 2 being within 2% seems insignificant. In addition, the prediction of case 2 compared with the experimental data has an error within 4.5%. For other operation conditions, the error scales due to neglect may be different
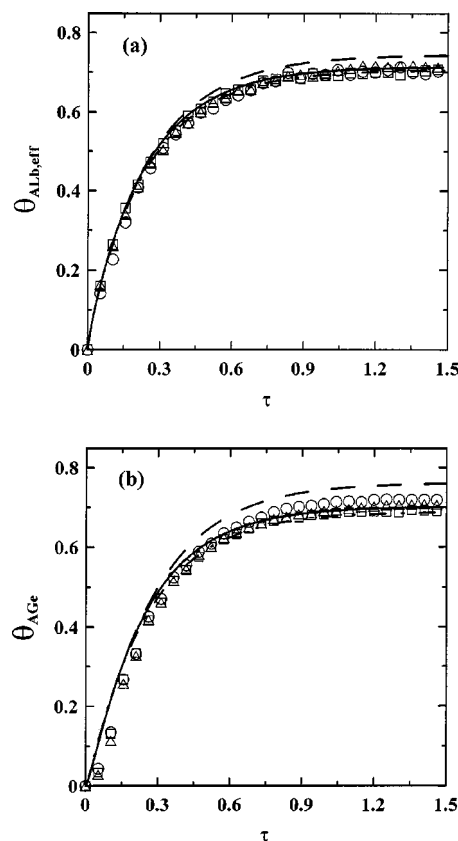
Fig. 1. $\theta_{ALb,eff}$ and θ_{AGe} versus τ for ozone dissolution in countercurrent bubble column. $u_L = 1.42$ mm/s. $u_{G0} = 1.33$ mm/s. $P_L = 0.221$, $St_{GA} = 1.54$, $St_{GO} = 0.215$, $Da_A = 0.1374$, $R_{uGL} = 215.1$, $R_{LF} = 11.62$, $\alpha_P = 0.128$. Symbols: experiments; lines: prediction. $\bigcirc$, $\triangle$, $\square$: $y_A = 0.00428, 0.0115, 0.0191$. ——, –·–, – –: DADM with cases 1, 2, and 3. Case 1: considers (1) oxygen mass transfer, and (2) u_G variation; case 2: neglects (1) while considers (2); and case 3: neglects both (1) and (2). (a) $\theta_{ALb,eff}$; (b) θ_{AGe}.

depending on the geometry, flow, mixing, and reactive regime. However, an examination of previous studies (Zhou et al. 1994; Huang et al. 1998) indicates that the prediction of the dissolved ozone concentration profile at steady state without considering the oxygen mass transfer is satisfactorily close to the experimental data. One may propose that the oxygen mass transfer may be neglected for simulation of the ozone concentration with respect to engineering applications. Note that the dissolved oxygen concentrations cannot be obtained from cases 2 and 3 assuming oxygen as an inert gas. There is a time lag of about $0.05t_L$ for θ_{AGe} between the experimental data and model predictions due to the nonideal complete mixing condition of the free volume. The results indicate that the variation of the superficial gas velocity had better be considered, while the oxygen mass transfer may be neglected for the ozone concentration estimation.

$U_{G,\zeta=1}$ represents the amount of the off-gas that can be used for computing the ozone transfer efficiency (η_{OTE}) and specific transferred ozone dosage (m_{STOD}). η_{OTE} is defined as the percentage of inlet ozone transferred into target water. That is,

$$\eta_{OTE} = \frac{u_{G0}C_{AGi0} - u_{G,z=L}C_{AGi,z=L}}{u_{G0}C_{AGi0}} = 1 - U_{G,\zeta=1}\theta_{AGi,\zeta=1}$$

(17)

m_{STOD} is defined as ratio of transferred ozone, in moles or milligrams, to the target water volume, in cubic meters and liters. That is,
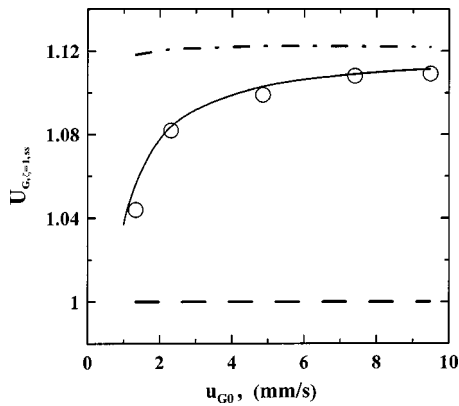
Fig. 2. $U_{G,\zeta=1}$ versus u_{G0} at steady state for ozone dissolution in countercurrent bubble column. $u_L = 4.25$ mm/s. $y_A = 0.020$. Symbols: experiments; lines: prediction. ——, –·–, – –: DADM with cases 1, 2, and 3 as specified in Fig. 1.

$$m_{STOD} = m_{SAOD} \times \eta_{OTE} = \frac{u_{G0} C_{AGi0}}{u_L} (1 - U_{G,\zeta=1} \theta_{AGi,\zeta=1}) \tag{18}$$

where m_{SAOD} = specific applied ozone dosage = $C_{AGi0} \times u_{G0} \times A/(u_L \times A)$. Note that the values of η_{OTE} and m_{STOD} decrease with the ozone contacting time until reaching steady state due to variations of $U_{G,\zeta=1}$ and $\theta_{AGi,\zeta=1}$. The steady-state values of $U_{G,\zeta=1}$ predicted by the model simulations for the three cases are compared with the experimental data, as shown in Fig. 2. It is seen that the prediction of case 1 indicates a good agreement. The value of $U_{G,\zeta=1}$ increases with u_{G0}, and approaches a constant at high u_{G0}. In contrast, cases 2 and 3 overestimate and underestimate the values of $U_{G,\zeta=1}$, respectively. Consequently, consideration of the oxygen mass transfer and superficial gas velocity variation gives an accurate computation of $U_{G,\zeta=1}$.

To further verify the validity of DADM, ozone dissolution experiments with various u_{G0} are performed and compared with the model prediction, as shown in Fig. 3, indicating good agreements. All the concentrations ($\theta_{ALb,eff}$, θ_{AGe}, and $\theta_{OLb,eff}$) with higher u_{G0} reach steady state faster due to higher volumetric mass transfer coefficients ($k_{LA}^0 a$ and $k_{LO}^0 a$, as indicated in Table 1). Further, a higher u_{G0} gives higher dimensionless concentrations. The predicted concentration profiles of θ_{ALb} in the bubble column at $\tau = 0.2$, 0.5, 1.0, and steady state for $u_{G0} = 1.33$ and 9.48 mm/s are shown in Fig. 4. It is seen that the shapes of the concentration profiles in the transient state are similar to those in the steady state. The value of $\theta_{ALb}/\theta_{ALb,ss}$ decreases with the axial coordinate (ζ) from the bottom to the top of the column. Therefore, the dissolved ozone concentration near the bottom of the column approaches the steady state faster.

To show the effects of various dimensionless parameters on the dynamic process of the ozone dissolution in a countercurrent bubble column, Figs. 5–7 depict the time variations of $\theta_{ALb}/\theta_{ALb,ss}$ of the effluent at different levels of P_L, Da_A, and $k_{LO}^0 a$, respectively. Note that the effects of $k_{LA}^0 a$, St_G, and St_L on the transient state are reflected by $k_{LO}^0 a$ in Fig. 7, as they are proportional to $k_{LO}^0 a$. The following conditions for the column are assigned as the base values: $y_A = 0.0115$, $y_O = 0.9885$, $Da_A = 0.0458$, $Da_O = 0.00648$, $k_{LO}^0 a = 0.00664$ s^{-1}, $P_G = 500$, $P_L = 10.0$, $St_{GA} = 1.55$, $St_{GO} = 0.216$, $St_{LA} = 1.84$, $St_{LO} = 2.08$, $\alpha_P = 0.128$, and $R_{uGL} = 71.3$. It is apparent that the approach to the steady state of $\theta_{ALb,eff}$ is accelerated by increasing the values of
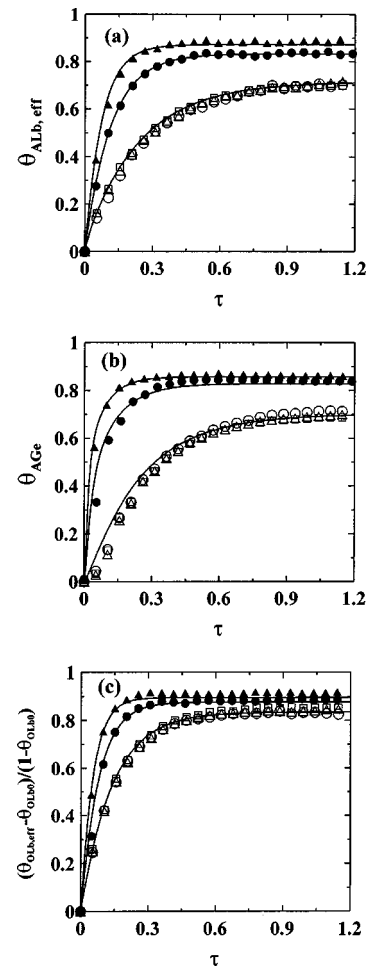
Fig. 3. $\theta_{ALb,eff}$, θ_{AGe}, and $(\theta_{OLb,eff} - \theta_{OLb0})/(1 - \theta_{OLb0})$ versus τ for ozone dissolution in countercurrent bubble column. $u_L = 1.42$ mm/s. Symbols: experiments; lines: prediction. ○, △, □: $y_A = 0.00428$, 0.0115, and 0.0191 at $u_{G0} = 1.33$ mm/s. ●: $y_A = 0.0192$ at $u_{G0} = 4.85$ mm/s. ▲: $y_A = 0.0162$ at $u_{G0} = 9.48$ mm/s. (a) $\theta_{ALb,eff}$, (b) θ_{AGe}, and (c) $(\theta_{OLb,eff} - \theta_{OLb0})/(1 - \theta_{OLb0})$.

P_L, Da_A, and $k_{LO}^0 a$. As P_L increases, the system approaches plug flow and has a higher axial gradient of θ_{ALb} and driving force of the concentration difference. This is favorable to the gas–liquid mass transfer. Further, the values of θ_{ALb} at steady state decrease as Da_A increase. The higher decomposition rate of ozone is thus advantageous to reaching steady state. Moreover, an increase of the mass transfer rate of ozone associated with an increase of $k_{LA}^0 a$, which is proportional to $k_{LO}^0 a$, results in an increase of θ_{ALb}, accelerating the establishment of the steady state. These results demonstrate that the DADM proposed in this study is useful and referable for the prediction and illustration of dynamic ozone contacting processes.

Conclusions

1. The model proposed considers the oxygen mass transfer as well as the superficial gas velocity (U_G) variation. The dynamic variations of the ozone and oxygen concentrations during ozone dissolution in a countercurrent bubble column can be well predicted from the beginning to steady state.

JOURNAL OF ENVIRONMENTAL ENGINEERING / NOVEMBER 2002 / **1041**
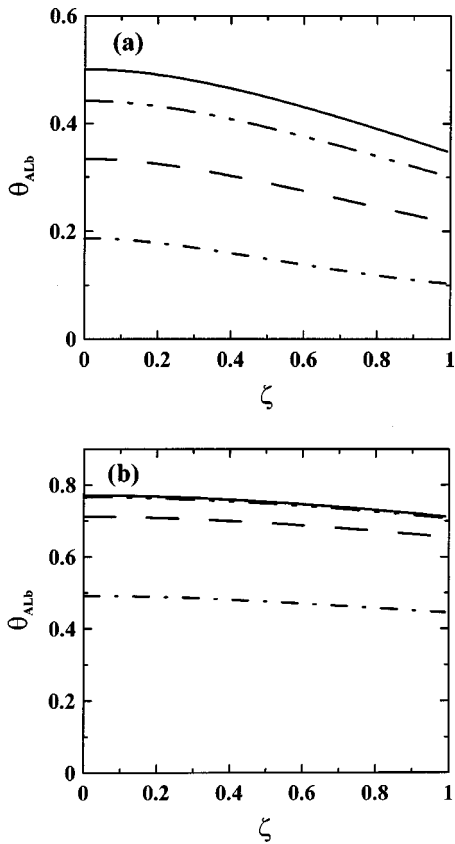
Fig. 4. θ_{ALb} versus ζ for ozone dissolution in countercurrent bubble column. $u_L = 4.25$ mm/s. $y_A = 0.0115$. Lines: prediction. $-\cdot-$, $--$, $-\cdot\cdot-$, and $——$: $\tau = 0.2$, 0.5, and 1.0, and steady state. (a) $u_{G0} = 1.33$ mm/s; and (b) $u_{G0} = 9.48$ mm/s.

2. For engineering application, the oxygen mass transfer may be neglected for simulation of ozone concentrations. The corresponding errors compared with experimental data are found $< 4.5\%$ in this study. However, correction of U_G associated with the hydraulic pressure should be considered. Otherwise, $4–10\%$ of overestimation would result.
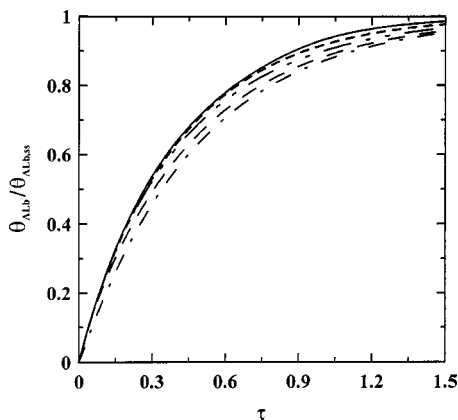
Fig. 5. $\theta_{ALb}/\theta_{ALb,ss}$ of effluent versus τ at various P_L for ozone dissolution in countercurrent bubble column. Lines: prediction. $-\cdot-$, $--$, $-\cdot\cdot-$, $-------$, and $——$: $\mathsf{P}_L = 0.01$, 0.667, 2.5, 10, and 100 (with $\theta_{ALb,ss} = 0.462$, 0.501, 0.559, 0.619, and 0.653).
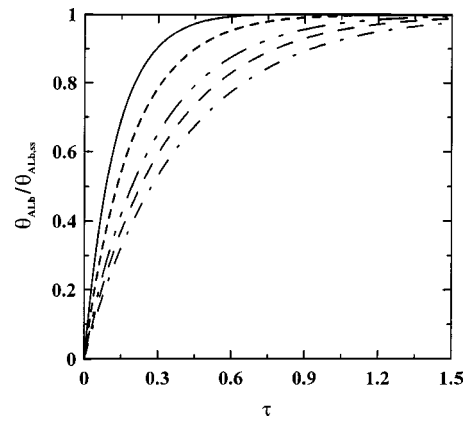
Fig. 6. $\theta_{ALb}/\theta_{ALb,ss}$ of effluent versus τ at various Da_A for ozone dissolution in countercurrent bubble column. Lines: prediction. $-\cdot-$, $--$, $-\cdot\cdot-$, $-------$, and $——$: $\mathsf{Da}_A = 0.0458$, 0.5, 1.0, 2.5, and 5.0 (with $\theta_{ALb,ss} = 0.619$, 0.523, 0.448, 0.314, and 0.211).

3. Both the oxygen mass transfer and U_G variation should be considered for accurate estimation of the amount of off-gas, which is related to the computation of the ozone transfer efficiency and specific transferred ozone dosage.
4. The higher value of U_G increases the saturation concentrations of the dissolved ozone and oxygen and the rate of the steady-state establishment owing to the higher mass transfer coefficients. On the contrary, the ozone transfer efficiency decreases with U_G. Further, the dissolved ozone concentration near the bottom of the column approaches the steady state faster.
5. The ozone contacting process in countercurrent bubble columns reaches the steady state faster with higher values of the Peclet number, ozone decomposition rate, and mass transfer rate.
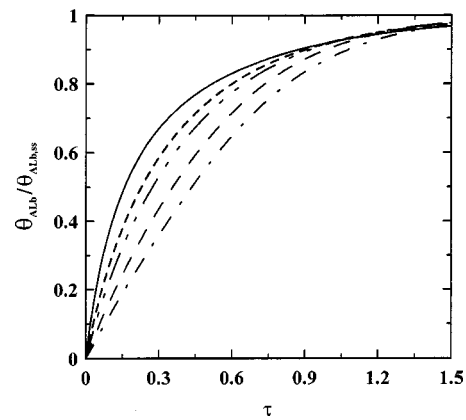
Fig. 7. $\theta_{ALb}/\theta_{ALb,ss}$ of effluent versus τ at various $k_{LO}^0 a$ for ozone dissolution in countercurrent bubble column. Lines: prediction. $-\cdot-$, $--$, $-\cdot\cdot-$, $-------$, and $——$: $k_{LO}^0 a = 0.001^a$, 0.003^b, 0.00664^c, 0.01^d, 0.02^e (with $\theta_{ALb,ss} = 0.203$, 0.431, 0.619, 0.702, and 0.808). (a) $k_{LA}^0 a = 0.000886$, $\mathsf{St}_{GO} = 0.0325$, $\mathsf{St}_{LO} = 0.313$, $\mathsf{St}_{GA} = 0.233$, $\mathsf{St}_{LA} = 0.277$. (b) $k_{LA}^0 a = 0.00266$, $\mathsf{St}_{GO} = 0.0975$, $\mathsf{St}_{LO} = 0.939$, $\mathsf{St}_{GA} = 0.699$, $\mathsf{St}_{LA} = 0.832$. (c) $k_{LA}^0 a = 0.00589$, $\mathsf{St}_{GO} = 0.216$, $\mathsf{St}_{LO} = 2.08$, $\mathsf{St}_{GA} = 1.55$, $\mathsf{St}_{LA} = 1.84$. (d) $k_{LA}^0 a = 0.00886$, $\mathsf{St}_{GO} = 0.325$, $\mathsf{St}_{LO} = 3.13$, $\mathsf{St}_{GA} = 2.33$, $\mathsf{St}_{LA} = 2.77$. (e) $k_{LA}^0 a = 0.0177$, $\mathsf{St}_{GO} = 0.649$, $\mathsf{St}_{LO} = 6.26$, $\mathsf{St}_{GA} = 4.66$, $\mathsf{St}_{LA} = 5.55$.

Acknowledgment

Appendix: Mathematical Model and Derivation

With the decomposition of ozone and formation of oxygen, the mass transfer rates of ozone (A) and oxygen (O) may be enhanced and retarded, respectively. The ratios of the mass transfer rates with the decomposition of ozone and formation of oxygen to that without may be signed by the enhancement factor of the ozone decomposition (E_{rA}) and retarding factor of the oxygen formation (R_{fO}), respectively. According to the film model (Danckwerts 1970), the E_{rA} of ozone and R_{fO} of oxygen can be expressed as in Eqs. (19) and (20):

$$E_{rA} = \frac{\mathsf{Ha}}{\sinh \mathsf{Ha}} \frac{(C_{AGi}/H_A)\cosh \mathsf{Ha} - C_{ALb}}{C_{AGi}/H_A - C_{ALb}} \quad (19)$$

$$R_{fO} = 1 - \frac{3}{2}\frac{D_A}{D_O}\left[\frac{\mathsf{Ha}}{\sinh \mathsf{Ha}}\left(\frac{C_{AGi}}{H_A}\cosh \mathsf{Ha} - C_{ALb}\right) - \left(\frac{C_{AGi}}{H_A}\right.\right.$$

$$\left.\left. - C_{ALb}\right)\right] \Bigg/ \left(\frac{C_{OGi}}{H_O} - C_{OLb}\right) \quad (20)$$

with $\mathsf{Ha} = \sqrt{k_d D_A}/k_{LA}^0$. The common value of k_{LA}^0 is in the order of $2-3\times10^{-3}$ m/s (Langlais et al. 1991). The D_A in water is determined as 1.76×10^{-9} m²/s at 21°C. Substitution of these values and k_d allows one to calculate the value of Ha. Accordingly, the values of E_{rA} and R_{fO} can then be estimated from Eqs. (19) and (20), which are significantly different from unity only when k_d is greater than the magnitude of $200\ \text{s}^{-1}$ (where $\mathsf{Ha} \geqslant 0.3$). Qiu et al. (2001) found that the value of k_d obtained for their experimental conditions increases from 2×10^{-5} to $2\ \text{s}^{-1}$ in the pH range of 2 to 12. Thus, the values of E_{rA} and R_{fO} calculated are about $1-1.000002$ and $1-0.99993$ for the conditions examined in this study and can be reasonably taken as unity for the common cases of the ozone self-decomposition. Should the experimental conditions give the values of $\mathsf{Ha} > 0.3$, then one would have to perform the computation of E_{rA} and R_{fO} as noted in the present model.

The system variables of interest include the gas velocity, and gas and liquid concentration profiles. Assumptions of the model may be deemed properly as follows (Mariñas et al. 1993; Zhou et al. 1994; Huang et al. 1998):

1. For the homogeneous bubbling flow regime, the dispersion coefficients, gas holdup, and mass transfer coefficients are constant along the height of the column;
2. The end effect of the column can be neglected;
3. Pressure varies linearly with the column height owing to the hydrostatic head;
4. Henry's law applies; and
5. Chemical reactions in gas phase are neglected.

Based on the above assumptions, the overall mass balance of gas phase may be described by Eq. (21). The left-hand-side term represents the variation of the local gas concentration, while the right-hand-side terms stand for the dispersion effect, convection, and ozone and oxygen mass transfers, respectively.

$$\varepsilon_G \frac{\partial C_G}{\partial t} = \varepsilon_G E_G \frac{\partial^2 C_G}{\partial z^2} - \frac{\partial(u_G C_G)}{\partial z} - E_{rA}k_{LA}^0 a\left(\frac{C_{AGi}}{H_A} - C_{ALb}\right)$$

$$- R_{fO}k_{LO}^0 a\left(\frac{C_{OGi}}{H_O} - C_{OLb}\right) \quad (21)$$

Applying the ideal gas equation and noting that the hydrostatic pressure (P) decreases linearly with the axial coordinate from the bottom of the column, one has

$$C_G = \frac{P}{RT} = \frac{P_T + \varepsilon_L \rho_L g(L-z)/f_P}{RT} = \frac{P_T \beta_P}{RT} \quad (22)$$

with $\beta_P = 1 + \alpha_P(1 - z/L)$, and $\alpha_P = \varepsilon_L \rho_L gL/(f_P P_T)$.

Substituting Eq. (22) into Eq. (21), and putting in dimensionless forms, one may obtain Eq. (3) of the dimensionless superficial gas velocity (U_G) and the related Eqs. (4)–(6). While the bubbles rise along the axial coordinate of the column, the liquid height (L) also increases due to the accumulation of the gas holdup. The increased L tends to be constant as the gas bubbles reach the liquid surface. Steady state L is considered to be equal to $L_0/(1-\varepsilon_G)$, where L_0 is the liquid height with no gas holdup.

Further, the gas phase governing equations of ozone (C_{AGi}) and oxygen (C_{OGi}) can be expressed in dimensionless forms (7) and (8). The liquid phase governing the equations of ozone (C_{ALb}) and oxygen (C_{OLb}) should consider ozone decomposition terms according to Eq. (2) to give Eqs. (9) and (10). The gas ozone concentration (C_{AGe}) in the free volume (V_F) in a bubble column can be described by Eq. (11) with the complete mixing assumption. The dimensionless variables and parameter groups in the system equations are defined in the Notation. Note that the Peclet numbers represent the flow condition. As the values of Peclet numbers become large, the system tends to approach plug flow. For small values of the Peclet numbers, the flow would behave as in complete mixing. Furthermore, the Stanton and Damköhler numbers stand for the significance of the mass transfer and chemical reaction, respectively.

Notation

The following symbols are used in this paper:

A = cross section area of column (m²);

a = specific gas–liquid interfacial area based on volume of liquid and gas (1/m);

$C_{AGe}, C_{AGe,ss}$ = gas concentration of ozone in free volume and its steady-state value (M or mg/L);

C_{AGi}, C_{AGi0} = gas concentrations of ozone of holdup and inlet gases (M or mg/L);

$C_{ALb}, C_{ALb,eff}$ = dissolved ozone concentrations in bulk and effluent liquids (M or mg/L);

$C_{ALb,ss}$ = steady-state value of C_{ALb} (M or mg/L);

C_{ALi} = dissolved ozone concentration of liquid at gas–liquid interface (M or mg/L);

$C_e, \overline{C_e}$ = experimental concentration data and its average value (M or mg/L);

C_G = total gas concentration in gas phase (M or mg/L);

C_{OGi}, C_{OGi0} = gas concentrations of oxygen of holdup and inlet gases (M or mg/L);

$C_{OLb}, C_{OLb,eff}$ = dissolved oxygen concentrations in bulk and effluent liquids (M or mg/L);

$C_{OLb0}, C_{OLb,ss}$ = C_{OLb} at initial time and steady state (M or mg/L);

C_{OLi} = dissolved oxygen concentration of liquid at gas–liquid interface (M or mg/L);

C_p = predicted concentration values (M or mg/L);

C_t = tracer concentration (mg/L);

C_θ = dimensionless concentration of tracer $= C_t Q_L \tau_L / m_t$;

D_A, D_O = molecular liquid diffusion coefficients of ozone and oxygen (m²/s);

Da_A, Da_O = Damköhler numbers of ozone $(= \varepsilon_L k_d L / u_L)$ and oxygen $[= 3\varepsilon_L k_d L C_{AGi0} H_O / (2u_L C_{OGi0} H_A)]$;

E_G, E_L = gas and liquid axial dispersion coefficients (m²/s);

E_{rA} = enhancement factor of ozone defined as in Eq. (19);

f_P = unit converted factor of pressure $= 101\ 325$ Pa (atm)$^{-1}$;

g = standard acceleration of gravity $= 9.8$ m/s²;

H_A, H_O = Henry's law constants of ozone $(= C_{AGi}/C_{ALi})$ and oxygen $(= C_{OGi}/C_{OLi})$ (M M^{-1});

Ha = dimensionless Hatta number, $= \sqrt{k_d D_A}/k_{LA}^0$;

h_B, h_B^* = dimensional (m) and dimensionless ($h_B^* = h_B/L$) heights of rising gas bubbles at time t;

h_s = hydrostatic height of two different positions for estimating ε_G, $\varepsilon_G = \Delta P/[(\rho_L - \rho_G)gh_s]$ (m);

k_d = decomposition rate constant of ozone (1/s);

k_{LA}^0, k_{LO}^0 = physical liquid-phase mass transfer coefficients of ozone and oxygen (m/s);

$(k_{LA}^0 a)_{sb}$ = value of $k_{LA}^0 a$ in semibatch reactor (1/s);

L, L_0 = liquid heights at steady state, or with no gas holdup (m);

m_{SAOD} = specific applied ozone dosage, $= C_{AGi0} \times u_{G0} \times A / (u_L \times A)$ (mg/L);

m_{STOD} = specific transferred ozone dosage defined as (18) (mg/L);

m_t = injection tracer mass (mg);

NLPM = L/min at 0°C, 1 atm;

P = hydrostatic pressure as function of location of column in Eq. (22) (atm);

P_T = gas pressure at free space (atm or kPa);

P_{z_M} = P at position z_M (kPa);

P_G, P_L = Peclet numbers of gas $[= u_{G0}L/(E_G \varepsilon_G)]$ and liquid $[= u_L L/(E_L \varepsilon_L)]$ phases;

Q_L = liquid flow rate (L/s);

R = gas constant, $= 0.082$ atm L K^{-1} mol^{-1};

R_{fO} = retarding factor of oxygen defined as in Eq. (20);

R_{LF} = ratio of modified volume of liquid to free space, $= A\varepsilon_L L u_{G0}/(V_F u_L)$;

R_{uGL} = gas–liquid velocity ratio, $= u_{G0}\varepsilon_L/(u_L \varepsilon_G)$;

R^2 = determination coefficient, $1 - [\Sigma(C_e - C_p)^2 / \Sigma(C_e - \overline{C_e})^2]$;

r^2 = correlation coefficient;

St_{GA}, St_{GO} = gas Stanton numbers of ozone $[= k_{LA}^0 aL/(u_{G0}H_A)]$ and oxygen $[= k_{LO}^0 aL/(u_{G0}H_O)]$;

St_{LA}, St_{LO} = liquid Stanton numbers of ozone $(= k_{LA}^0 aL/u_L)$ and oxygen $(= k_{LO}^0 aL/u_L)$;

T = temperature (K);

t, t_c = time (s), and contact time (min or s);

t_L = mean liquid phase residence time, $= L\varepsilon_L/u_L$ (min or s).

t_{10} = time for 10% of tracer mass to exit column (min or s);

U_G, $U_{G,\zeta=1}$, $U_{G,\zeta=1,ss}$ = u_G/u_{G0}, $u_{G,z=L}/u_{G0}$, and $U_{G,\zeta=1}$ at steady state;

u_G, u_L = superficial gas and liquid velocities (m/s or mm/s);

$u_{G,z=L}$, u_{G0} = outlet and inlet superficial gas velocities (m/s or mm/s);

V_F = volume of free space (m³ or L);

y_A, y_O = mole fractions of ozone and oxygen of inlet gas;

z = axial coordinate of column from bottom (m);

z_M = z at position M near middle of column (m);

α_P = pressure ratio, $= \varepsilon_L \rho_L g L / (f_P P_T)$;

β_P = local variable, $= 1 + \alpha_P(1 - z/L)$;

$\delta(\tau)$ = Dirac delta function to represent discontinuous pulse;

ΔP = pressure difference between two positions with and without aeration of hydrostatic height h_s for estimating ε_G, $\varepsilon_G = \Delta P/[(\rho_L - \rho_G)gh_s]$ (Pa);

ε_G, ε_L = relative gas and liquid holdups;

η_{OTE} = ozone transfer efficiency defined as in Eq. (17);

θ_{AGi}, θ_{AGe} = C_{AGi}/C_{AGi0}, C_{AGe}/C_{AGi0};

θ_{ALb}, $\theta_{ALb,eff}$, $\theta_{ALb,ss}$ = $C_{ALb}/(C_{AGi0}/H_A)$, $C_{ALb,eff}/(C_{AGi0}/H_A)$, and steady-state value of θ_{ALb};

θ_{OGi} = dimensionless C_{OGi}, C_{OGi}/C_{OGi0};

θ_{OLb}, $\theta_{OLb,eff}$, θ_{OLb0} = $C_{OLb}/(C_{OGi0}/H_O)$, $C_{OLb,eff}/(C_{OGi0}/H_O)$, and $C_{OLb0}/(C_{OGi0}/H_O)$;

μ_L = liquid viscosity (kg m^{-1} s^{-1});

ρ_G, ρ_L = gas and liquid densities (kg/m³);

σ_L = liquid surface tension (N/m);

τ = dimensionless time, $= t/t_L$; and

ζ = dimensionless axial coordinate of column from bottom, $= z/L$.

Subscripts

sb = semibatch stirred reactor; and

ss = steady state.

References

Akita, K., and Yoshida, F. (1973). "Gas holdup and volumetric mass transfer coefficient in bubble columns." *Ind. Eng. Chem. Process Des. Dev.,* 12(1), 76–80.

Alvarez-Cuenca, M., and Nerenberg, M. A. (1981). "Oxygen mass transfer in bubble columns working at large gas and liquid flow rates." *AIChE J.,* 27(1), 66–73.

Biń, A. K. (1995). "Application of a single-bubble model in estimation of ozone transfer efficiency in water." *Ozone. Sci. Eng.,* 17(5), 469–484.

Chang, C. Y., et al. (2001). "Kinetics of decomposition of polyethylene glycol in electroplating solution by ozonation with UV radiation." *J. Environ. Eng.,* 127(10), 908–915.

Chiu, C. Y., et al. (1997). "A refined model for ozone mass transfer in a semibatch stirred vessel." *Ozone. Sci. Eng.,* 19(5), 439–456.

Chiu, C. Y., Chang, C. Y., Chen, Y. H., Yu, Y. H., Chiang, P. C., and Ku, Y. (2002). "Ozone mass transfer with combined effects of ozone de-

composition and reaction with pollutants in a semibatch stirred vessel." *J. Chin. Inst. Chem. Eng.*, in press.

Danckwerts, P. V. (1970). *Gas–liquid reactions*, 1st Ed., McGraw-Hill, New York.

Deckwer, W. D., Burckhart, R., and Zoll, G. (1974). "Mixing and mass transfer in tall bubble columns." *Chem. Eng. Sci.,* 29, 2177–2188.

Deckwer, W. D., Nguyen-Tien, K., Kelkar, B. G., and Shah, Y. T. (1983). "Applicability of axial dispersion model to analyze mass transfer measurements in bubble columns." *AIChE J.,* 29(6), 915–922.

Deckwer, W. D., and Schumpe, A. (1993). "Improved tools for bubble column reactor design and scale-up." *Chem. Eng. Sci.,* 48(5), 889–911.

Hikita, H., Asai, S., Tanigawa, K., Segawa, K., and Kitao, M. (1981). "The volumetric liquid-phase mass transfer coefficient in bubble columns." *Chem. Eng. J.,* 22, 61–69.

Huang, W. H., et al. (1998). "A refined model for ozone mass transfer in a bubble column." *J. Environ. Sci. Health, Part A: Toxic/Hazard. Subst. Environ. Eng.,* 33(3), 441–460.

Kuo, C. H., and Huang, C. H. (1995). "Aqueous phase ozonation of cholorophenols." *J. Haz. Mat.,* 41, 31–45.

Langlais, B., Reckhow, D. A., and Brink, D. R. (1991). *Ozone in water treatment application and engineering*, 1st Ed., Lewis, Mich.

Le Sauze, N., Laplanche, A., Martin, N., and Martin, G. (1993). "Modeling of ozone transfer in a bubble column." *Water Res.,* 27(6), 1071–1083.

Letzel, H. M., Schouten, J. C., Krishna, R., and Van den Bleek, C. M. (1999). "Gas holdup and mass transfer in bubble column reactors operated at elevated pressure." *Chem. Eng. Sci.,* 54(13–14), 2237–2246.

Levenspiel, O. (1972). *Chemical reaction engineering*, 2nd Ed., Wiley, New York.

Li, H., et al. (2000). "Kinetics of ozonation of polyethylene glycol in printed wiring board electroplating solution." *J. Chin. Inst. Environ. Eng. (Taiwan),* 10(1), 69–75.

Mariñas, B. J., Liang, S., and Aieta, E. M. (1993). "Modeling hydrodynamics and ozone residual distribution in a pilot-scale ozone bubble-diffuser contactor." *J. Am. Water Works Assoc.,* 85(3), 90–99.

Masschelein, W. J. (1982). *Ozonization manual for water and wastewater treatment*, 1st Ed., Wiley, New York.

McGhee, T. J. (1991). *Water supply and sewerage*, 6th Ed., McGraw-Hill, New York.

Qiu, Y., Kuo, C. H., and Zappi, M. E. (2001). "Performance and simulation of ozone adsorption and reaction in a stirred-tank reactor." *Environ. Sci. Technol.,* 35(1), 209–215.

Rankness, K., et al. (1996). "Guideline for measurement of ozone concentration in the process gas from an ozone generator." *Ozone. Sci. Eng.,* 18(3), 209–229.

Rice, R. G., Tupperainen, J. M. I., and Hedge, R. M. (1981). "Dispersion and hold-up in bubble columns—Comparison of rigid and flexible spargers." *Can. J. Chem. Eng.,* 59(6), 677–687.

Sawyer, C. N., McCarty, P. L., and Parkin, G. F. (1994). *Chemistry for environmental engineering*, 4th Ed., McGraw-Hill, New York.

Shah, Y. T., Kelkar, B. G., Godbole, S. P., and Deckwer, W. D. (1982). "Design parameters estimations for bubble column reactors." *AIChE J.,* 28(3), 353–379.

Shetty, S. A., Kantak, M. V., and Kelkar, B. G. (1992). "Gas-phase back-mixing in bubble-column reactors." *AIChE J.,* 38(7), 1013–1026.

Smith, D. W., and Zhou, H. (1994). "Theoretical analysis of ozone distribution performance in a bubble column." *Ozone. Sci. Eng.,* 16(5), 429–441.

Sotelo, J. L., Beltrán, F. J., Benítez, F. J., and Beltrán-Heredia, J. (1989). "Henry's law constant for the ozone–water system." *Water Res.,* 23(10), 1239–1246.

Staehelin, J., and Hoigné, J. (1982). "Decomposition of ozone in water: Rate of initial by hydroxide ions and hydrogen peroxide." *Environ. Sci. Technol.,* 16(10), 676–681.

Wilke, C. R., and Chang, P. C. (1955). "Correlations of diffusion coefficients in dilute solutions." *AIChE J.,* 1, 264–270.

Wright, P. C., Meeyoo, V., and Soh, W. K. (1998). "A study of ozone mass transfer in a cocurrent downflow jet pump contactor." *Ozone. Sci. Eng.,* 20(1), 17–33.

Zahradník, J., and Fialová, M. (1996). "The effect of bubbling regime on gas and liquid phase mixing in bubble column reactors." *Chem. Eng. Sci.,* 51(10), 2491–2500.

Zhou, H., Smith, D. W., and Stanley, S. J. (1994). "Modeling of dissolved ozone concentration profiles in bubble columns." *J. Environ. Eng.,* 120(4), 821–840.